JCTC Journal of Chemical Theory and Computation

Coarse-Grained Computer Simulations of Polymer/Fullerene Bulk Heterojunctions for Organic Photovoltaic Applications

David M. Huang,* Roland Faller, Khanh Do, and Adam J. Moulé

Chemical Engineering and Materials Science Department, University of California, Davis, California 95616

Received September 17, 2009

Abstract: We develop coarse-grained (CG) computer simulation models of poly(3-hexyl-thiophene) (P3HT) and P3HT/fullerene-C_{60} mixtures, in which collections of atoms from a physically accurate atomistic model are mapped onto a smaller number of "superatoms". These CG models allow much larger systems to be simulated for longer durations than is achievable atomistically, making it possible to study in molecular detail the morphology of polymer/fullerene bulk heterojunctions at length and time scales relevant to organic photovoltaic devices. We demonstrate that our CG models, parametrized at two state points, accurately capture the structure of atomistic systems at other points in the mixture phase diagram. Finally, we use our CG models to study the dynamic evolution of the microstructure of a P3HT/C_{60} bulk heterojunction in a system approaching the device scale.

1. Introduction

Meeting the world's growing demand for energy with renewable, nonpolluting sources is one of the biggest challenges facing society.[1,2] Solar power is arguably the only source capable of supplying these needs into the next century.[3] But state-of-the-art crystalline silicon technology is currently not economically competitive with fossil fuels.[4] Organic photovoltaics (OPV), which includes polymer-based solar cells (PSCs), offers a cost-effective alternative to traditional crystalline silicon solar cells.[5] Advantages of OPV include solution processability, device flexibility, and the potential for high-volume reel-to-reel production, but device efficiencies must improve if OPV is to become commercially viable.[5]

Typical PSCs use a mixture of a light-absorbing semi-conducting polymer as the electron donor and a fullerene derivative as the electron acceptor in the solar cell's photoactive layer. Because of the large discrepancy between the exciton diffusion length ($\sim$5−10 nm)[6] in the donor and the optimal active layer thickness for light absorption (>100 nm), the donor and acceptor phases are usually mixed together to form a bicontinuous network called a bulk

heterojunction (BHJ),[7] in which generated excitons are (ideally) less than a diffusion length from a donor−acceptor interface. The delicate balance between maximizing interfacial area and maintaining percolating pathways for charge transport to the electrodes means that PSC device performance is sensitive to the BHJ morphology. Furthermore, the highly anisotropic nature of charge transport (e.g., intra- vs interchain or in the π-stacked vs side-chain direction) in semiconducting polymers[8] means that device efficiencies also depend on the molecular-scale organization of the donor and acceptor within the BHJ. Even with the same electron donor and acceptor materials, BHJ solar cell efficiencies can vary dramatically: for poly(3-hexylthiophene)/[6,6]-phenyl-C_{61}-butyric acid methyl ester (P3HT/PCBM) blends, one of the most widely used donor/acceptor combinations, varying the polymer chain length[9] and using processing steps such as heat tempering[10] and solvent soaking[11] can change device efficiencies from under 0.1% to the record efficiencies of $\sim$5% that have recently been achieved.[11−13]

The fabrication of BHJ polymer solar cells is currently more of an art than a science: despite the crucial importance of the heterojunction morphology for device performance, it is still not known how to predict the microstructure of the photoactive layer based on the constituent materials or

---

* Corresponding author e-mail: dmhuang@ucdavis.edu.

processing conditions. Although a wealth of nanoscale morphological information on semiconducting polymer thin films and BHJs has become available from experimental techniques such as X-ray diffraction,[14–26] atomic force microscopy,[21,24–27] transmission electron microscopy[24,25] and tomography,[28,29] optical spectroscopy,[17,23,24,30] spectroscopic ellipsometry,[30] and near-edge X-ray absorption fine structure (NEXAFS) spectroscopy,[30] the molecular-scale structure is not easily resolved by any of these methods and must usually be inferred indirectly. An unambiguous assignment of the structure is thus often not possible. The lack of long-range order in semiconductor polymer films further complicates data interpretation. The phase behavior of polymer/fullerene mixtures and its relationship to charge transport and device performance has also been investigated experimentally, but even for the same P3HT/PCBM blend, there is some disagreement between the published phase diagrams;[31,32] difficulties in interpreting the measured data make resolving these discrepancies a challenge.

Accurate computer simulation models can play an important role in elucidating the phase behavior of polymer/fullerene mixtures, the morphology of BHJs, and the influence of the morphology on charge transport; they can also aid the interpretation of experimental data, because particle positions can be tracked exactly during the course of a simulation. A number of atomistic computer simulation studies[8,33] have examined the molecular structure of organic semiconductors[34,35] and its effect on charge transport.[36–38] However, the computational demands of atomistic simulations mean that systems of only a few nanometers can be readily studied. The study of domains the size of the exciton diffusion length ($\sim$5−10 nm), the length scale of interest for charge transport in polymer solar cells, is thus computationally prohibitive by these methods.

Coarse-grained (CG) simulations,[39–43] in which collections of atoms from an atomistic model are mapped onto a smaller number of "superatoms", allow multiple domains the size of the exciton diffusion length to be studied while retaining significant information about the molecular structure, thereby allowing the BHJ morphology and its effect on charge transport (if the simulation model is coupled to a charge transport model[8]) to be analyzed on length scales relevant to polymer photovoltaics.

In this article, we develop CG models of poly(3-hexylthiophene) (P3HT), one of the most widely used semiconducting polymers in OPV, and C_{60}, the simplest fullerene, and mixtures of the two materials. (C_{60} is studied in this initial study because of its simplicity, but our future work will concentrate on PCBM, the fullerene most widely used in PSCs.) We use accurate atomistic force fields as the starting point for developing the CG models. We parametrize the CG interactions using simulations at 550 K and 1 atm to ensure that the simulated systems are in the fluid state and isotropic, because the nonbonded pair interactions are assumed to be isotropic in the CG models. We then verify that the CG models accurately capture the phase behavior of the atomistic models at various temperatures and mixture compositions. Finally we demonstrate that the CG models can be used to study the structure and dynamic evolution of
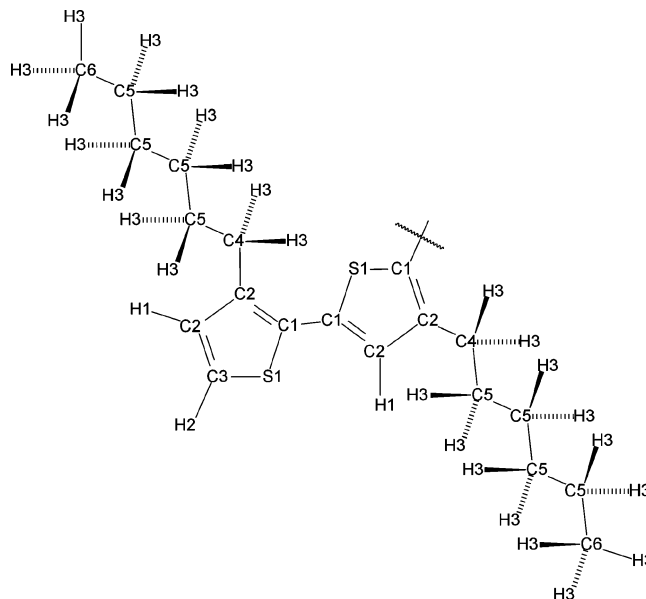

Figure 1. Chemical structure of last two monomers in a poly(3-hexylthiophene) (P3HT) chain. Atoms of different types in our atomistic model are labeled with different numerical suffixes.

the BHJ microstructure of polymer/fullerene mixtures for a system approaching the photovoltaic device scale and down to temperatures where phase separation is expected to occur.

2. Atomistic Simulation Models

The atomistic model of P3HT used in this work was adapted from the simulation model of tetrathiophene (T4) developed by Marcon and Raos[44] (which we will call the MR model from now on). The molecular geometry and atom types in our P3HT model are depicted in Figure 1. For the rest of this paper, we will focus on simulations of 100% regioregular P3HT (rr-P3HT), in which all monomers are joined head-to-tail; the models and methods presented in this paper are, however, equally applicable to P3HT with any degree of regioregularity.

Equilibrium distances and angles and partial charges on the atoms in the MR model were determined from ab initio density functional theory calculations.[44,45] In addition to Coulombic interactions between the point charge sites on the atoms, nonbonded atoms in the MR model also have van der Waals interactions described by the Lennard−Jones (LJ) potential, $V_{ij}^{LJ}(r) = 4\varepsilon_{ij}[(\sigma_{ij}/r)^{12} - (\sigma_{ij}/r)^6]$, truncated at a cutoff distance of 12 Å. The parameters for the LJ diameter σ_{ij} and interaction strength ε_{ij} in the MR model[44] were obtained from the OPLS-AA model,[46] in which heteronuclear interaction parameters are specified by the geometric mean of the homonuclear parameters, i.e., $\sigma_{ij} = (\sigma_{ii}\sigma_{jj})^{1/2}$ and $\varepsilon_{ij} = (\varepsilon_{ii}\varepsilon_{jj})^{1/2}$. As in the OPLS-AA model, atoms in the same molecule separated by more than three bonds have the same nonbonded interactions (LJ + Coulombic) with each other as atoms on different molecules, atoms separated by three bonds interact 1/2 as strongly, and atoms separated by one or two bonds have no nonbonded interactions with each other. The MR model has been found to give good agreement with experiment for the density, X-ray crystal structure, and heat of

sublimation of T4[44] and therefore provides a good basis for our P3HT model.

The thiophene monomers in the MR model are slightly asymmetric, due to the significant chain-end effects in T4, whereas the thiophene units far from the ends in poly-thiophene (PT) should have reflection symmetry. For the PT backbone in our P3HT model, we have therefore used averaged equilibrium bond lengths and angles and bond stretching and bending force constants from the central monomers in the MR model and the charges from the half of the central monomers closest to the central intermonomer bond. The very slight asymmetry of the monomers in the MR model means that these modifications are small and should not have any noticeable quantitative impact on the results from our model. The simulation parameters for the alkyl side chain were taken directly from the OPLS-AA model,[46] except for the charge on the C4 carbon (see Figure 1), which was fixed by the requirement of monomer charge neutrality. The resulting partial charge of 0.0617e, where e is the elementary charge unit, is only slightly different from that of the equivalent site type (CH_2 bonded to aromatic C) of −0.005e in the OPLS-AA model. Marcon and Raos[45] used a similar strategy to determine the charge on the alkyl carbon directly bonded to the thiophene ring for their model of sexithiophene and tetrahexylsexithiophene, which were found to give reasonable agreement with experiment for the density and X-ray crystal structure.[45] The charges on the terminal carbon and hydrogen on the terminal monomers were adapted from those of the equivalent sites in the MR model,[44] with equal charges added to these two sites to ensure charge neutrality of the terminal monomers. The nonbonded, bond stretching, and bond bending parameters used in the atomistic simulation model of P3HT are given, respectively, in Tables S1−S3 in the Supporting Information.

All simulations, including the coarse-grained simulations described below, were carried out with the LAMMPS molecular dynamics simulation package.[47] Unless otherwise stated, electrostatic interactions were calculated using the particle−particle particle−mesh (PPPM) method.[48] C−H bond distances were constrained with the SHAKE algorithm.[49] All atomistic simulations were carried out at constant temperature and pressure (NPT ensemble), using a Nosé−Hoover thermostat[50] and Nosé−Hoover barostat.[51] A time-step of 1.5 to 2 fs was used, depending on the temperature.

High-level ab initio quantum calculations of bithiophene were used to determine the torsional potential of the intermonomer dihedral of T4 in the MR model,[52] in which constrained geometry optimizations and energy calculations were carried out at 30° intervals and the resulting points fit to a sixth-order cosine function. However, recent density functional theory calculations of thiophene and regioregular 3-hexylthiophene (3HT) oligomers[53] have shown substantial variations in the intermonomer torsional potential as a function of chain length, as shown in Figure 2 for 3HT dimers and 14-mers, with the potential only converging for chains 10 monomer units or longer. These variations were attributed to increasing electron delocalization with increasing chain length, making distortions of the chain from planarity less favorable for longer chains. Indeed, these recent calcula-
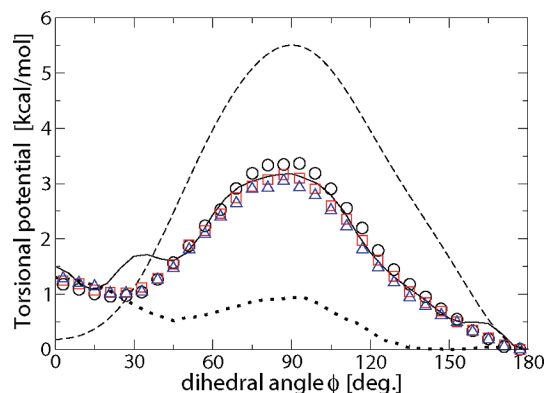

Figure 2. Intermonomer torsional potential for a 3HT 14-mer (solid line) and dimer (dotted line) as a function of S1−C1−C1−S1 dihedral angle ϕ (see Figure 1 for definition of atom types) from ab initio calculations in ref 53 ($\tilde{V}_{dihed}(\phi)$) and approximated as $-k_B T \ln P_{dihed}(\phi)$ from constant NVT simulations at 300 (circles), 400 (squares), and 500 K (triangles) of a single 3HT hexamer in the gas phase with the atomistic simulation model used in this work, with intrinsic torsional potential $V_{dihed}(\phi) = \sum_{i=0}^{8} c_i \cos^i(x)$ (dashed line), where $c_0 = 5.5121$, $c_1 = -0.0201$, $c_2 = -6.6011$, $c_3 = 1.1645$, $c_4 = 1.7991$, $c_5 = -5.1590$, $c_6 = 0.1496$, $c_7 = 4.1068$, and $c_8 = -0.7607$ kcal/mol.

tions show that, although the torsional potential of thiophene dimers and 3HT dimers has a global minimum at a dihedral angle ϕ of around 150°[52,53] and 135°,[53] respectively, the global minimum for 8-mers and larger is at 180°,[53] corresponding to a planar chain with monomers in the anti conformation. The local minimum at small dihedral angles corresponding to the syn conformer also moves to smaller angles for longer chains.[53] A planar structure is most consistent with the available experimental data: according to X-ray diffraction measurements of crystals of 3,4′,4″-trimethyl-2−2′:5′,2″-terthiophene (the trimer of regioregular 3-methylthiophene, which would be less sterically hindered than 3HT), the equilibrium dihedral angle is ~173°,[54] while similar measurements of rr-P3HT thin films also indicate a predominance of the planar conformation.[15]

We have therefore modeled the intermonomer torsional potential $\tilde{V}_{dihed}(\phi)$ in our atomistic model for P3HT using the ab initio torsional potential for the longest rr-3HT oligomer in ref 53, 3HT14, rather than using the bithiophene torsional potential in the MR model. The torsional potential calculations in ref 53 were carried out for rotations around the central intermonomer bond using rigid monomers whose atoms were fixed at their global minimum configuration and using a smaller basis set than the bithiophene calculations used in the MR model,[52] because of the computational expense of calculations of this nature for such large molecules. However, it is likely that the errors associated with the large chain length dependence of the torsional potential far outweigh those associated with the approximations used in these calculations. In fact, the torsional potential for bithiophene in ref 53 is quantitatively quite similar to that used in the MR model,[52] indicating that errors due to the smaller basis set, different level of theory, and rigid rotor approximation may be small. The ab initio intermonomer torsional potential $\tilde{V}_{dihed}(\phi)$ cannot be used directly in the simulation force field for our P3HT model because the model

Polymer/Fullerene Bulk Heterojunctions

J. Chem. Theory Comput., Vol. 6, No. 2, 2010 **529**

includes nonbonded (LJ + Coulombic) interactions that are implicitly contained in $\tilde{V}_{\text{dihed}}(\phi)$ in the ab initio calculations and which therefore must be subtracted from $\tilde{V}_{\text{dihed}}(\phi)$ to obtain the "intrinsic" torsional potential $V_{\text{dihed}}(\phi)$ that is used in the simulation force field. To account for the fact that the torsional potential of one dihedral angle depends on the orientation of more than just the adjacent monomers, we have determined an average torsional potential (in the "mean field" of monomers further along the chain) by carrying out constant NVT simulations of a single 3HT hexamer in the gas phase (longer chains gave indistinguishable results) at various temperatures and adjusting the intrinsic torsional potential $V_{\text{dihed}}(\phi)$ of the S1−C1−C1−S1 dihedral so that $-k_BT \ln P_{\text{dihed}}(\phi) \approx \tilde{V}_{\text{dihed}}(\phi)$, where $P_{\text{dihed}}(\phi)$ is the measured distribution of the central S1−C1−C1−S1 dihedral angle. (The torsional potentials of the C2−C1−C1−C2 and S1−C1−C1−C2 dihedrals were set to zero (see Figure 1 for the definitions of the atom types); other choices for the dihedral potentials, such as partitioning the total intrinsic torsional potential equally between the four dihedral angles, are not expected to affect results significantly.) Constant NVT simulations were carried out at 300, 400, and 500 K for 180, 36, and 18 ns, respectively. LJ and Coulombic interactions were truncated at a cutoff distance of 12 and 30 Å, respectively (the latter distance is larger than the molecule, so all Coulombic interactions were taken into account in this way). The intrinsic dihedral potential $V_{\text{dihed}}(\phi)$ was specified by an eighth-order cosine series, $V_{\text{dihed}}(\phi) = \sum_{i=0}^{8} c_i \cos^{i}(x)$. As shown in Figure 2, $-k_BT \ln P_{\text{dihed}}(\phi)$ is relatively insensitive to temperature over the 200 K range used in the simulations, indicating that it is reasonable to approximate this torsional potential energy function by what is actually a free energy. We did not attempt to fit the smaller bumps in the torsional potential for 3HT14 from ref 53 shown in Figure 2, which the authors of ref 53 concede may be an artifact of the rigid-rotor approximation used in their calculations. For the purposes of developing a coarse-grained model of P3HT, this level of accuracy, namely getting the positions of the minima in the potential and the barrier height approximately correct, is sufficient. Parameters for the torsional potentials for the alkyl side chains of P3HT were taken from the OPLS-AA model.[46,55]

Comparison of the results of simulations with our atomistic P3HT model with experimental data indicate that the model accurately represents the structure of P3HT. The monomer density (0.931 ± 0.003 g/mL) from a 0.7-ns constant NPT simulation of 256 3HT monomers at 298 K and 1 atm agrees well with the measured density (0.936 g/mL)[56] at the same thermodynamic conditions. The simulated density (1.05 g/cm³) from a constant NPT simulation of a crystal of 3HT 12-mers also agrees with the measured density (1.10 ± 0.05 g/cm³)[57] of P3HT thin films. (This simulation involved annealing at 1 atm an fcc lattice of 72 aligned chains all in the anti conformation from 400 to 298 K over 1 ns and then equilibrating at 298 K for another 1 ns, during which the density was measured.) Although a direct comparison between oligomer and polymer data is not strictly correct, the 3HT 12-mers studied should be long enough that the structure of the crystal is similar to that of long chains.

Unfortunately, experimental data that can be directly compared with our atomistic P3HT model is limited, because atomistic simulations of long P3HT chains, on which most experiments of P3HT morphology have focused, are not feasible; on the other hand, little experimental data exists for 3HT oligomers.

Turning to the atomistic model for C_{60}, the LJ parameters of the carbon atoms were taken from ref 58 and are given in Table S1 in the Supporting Information (the partial charges on the carbon atoms were all zero). The parameters in this model were obtained by computing the energy of an fcc crystal of C_{60} (treating the C_{60} molecule as a sphere with a surface of uniform density of carbon atoms) and comparing the results to experimental data for the heat of sublimation and lattice constant. The calculated compressibility from this model is close to the experimental value for an fcc crystal of C_{60}. The resulting parameters are also quite close to those in the OPLS-AA model for aromatic carbon atoms (see Table S1 in the Supporting Information),[46] indicating that combining our P3HT model (which uses OPLS-AA LJ parameters) with this C_{60} model should give reasonable results. The equilibrium bond lengths of C_{60} (see Table S2 in the Supporting Information) were taken from gas-phase electron diffraction measurements[59] and are consistent with the C_{60} diameter in ref 58. Given these bond lengths and C_{60}'s icosahedral geometry, the equilibrium bond angles (see Table S3 in the Supporting Information) and improper dihedral angles in C_{60} can readily be calculated. Harmonic improper dihedral potentials $V_{\text{improp}}(\xi) = k_\xi(\xi - \xi_0)^2/2$ were defined so as to maintain the icosahedral geometry of C_{60} and to maintain the planar geometry of the thiophene rings in P3HT. The force constant k_ξ was 40 kcal/mol/rad² in all cases.

3HT 12-mers (3HT12) were used in the atomistic simulations, as oligomers of this length have been shown previously[60,61] to behave sufficiently like long-chain polymers to be used in the coarse-graining procedure. The initial system configurations used in the simulations comprised random polymer chains and randomly placed fullerenes. An initial energy minimization of the system with soft nonbonded interaction potentials given by a truncated cosine function was used to eliminate particle overlaps. Simulations were carried for a total time of at least $6\tau_2$ and at least $9\tau_2$ for the simulations used to calculate distribution functions used in the optimization of the CG models, where τ_2 is a measure of the time scale for reorientation of the polymer chains and is obtained by fitting the autocorrelation function of the unit vector $\hat{\mathbf{u}}(t)$ between the polymer chain ends to the equation $\langle P_2[\hat{\mathbf{u}}(t)\cdot\hat{\mathbf{u}}(0)] \rangle \sim \exp(-t/\tau_2)$, where $P_2(x) \equiv (3x^2 - 1)/2$ is the second-order Legendre polynomial. Thus, total simulation times varied between around 5 and 35 ns. Mixtures with mole ratios that include those typically used in P3HT:PCBM solar cells were studied.[31] The thermodynamic conditions studied were chosen so as to include state points in the liquid phase and at or close to solid/liquid coexistence, based on the published experimental phase diagrams of P3HT:PCBM mixtures,[31,32] which are expected to exhibit solidification of the fullerene at a lower temperature than P3HT:C_{60} mixtures, due to the disordering effect of the PCBM side chain. (Unfortunately, to the best of our

Table 1. Temperatures and Mixture Ratios of Atomistic Systems Studied (pressure = 1 atm in all cases)[a]

n(3HT12)/n(C$_{60}$)	P3HT:C$_{60}$ (w/w)	P3HT:PCBM equiv[b] (w/w)	temperature (K)
60/0	1.00:0	1.0:0	500, 550, 650
50/55	2.52:1	2.0:1	550
48/72	1.85:1	1.5:1	550, 650
42/92	1.27:1	1.0:1	550, 650

[a] Regioregular P3HT (rr-P3HT) was used in all cases. [b] P3HT:PCBM mixture with same mole ratio as P3HT:C$_{60}$ mixture.
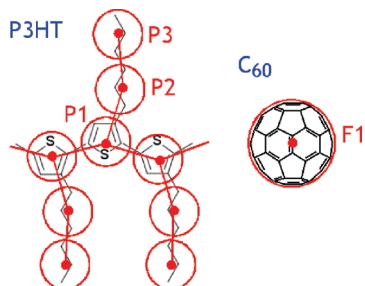
Figure 3. Chemical structures of P3HT and C$_{60}$ with coarse-grained sites depicted and labeled.

knowledge, no experimental phase diagram of P3HT:C$_{60}$ mixtures exists for a more direct comparison.) As a point of reference, the polymer/fullerene = 1:1 w/w composition is the mostly commonly used mixture in P3HT/PCBM photovoltaic devices, although it has been suggested that a 2:1 w/w composition is optimal.[31] Although desirable, it is challenging to simulate well-equilibrated atomistic systems under thermodynamic conditions far into regions of the phase diagrams in which solids exist, because of the computational expense of the atomistic simulations, and so we have limited the atomistic simulations to temperature above 500 K. CG simulations at lower temperatures are, however, feasible. Table 1 summarizes the various P3HT:C$_{60}$ mixture ratios and temperatures studied.

3. Coarse-Grained Models and Methods

Our strategy in designing coarse-grained (CG) models of P3HT and C$_{60}$ was to use the simplest models that would accurately capture the structure of these molecules. To this end, we modeled the P3HT monomer using three sites: (1) the center-of-mass (COM) of the thiophene ring and the COM of the carbon atoms of the (2) first three and (3) last three side-chain methyl groups. A single site, the molecule's COM, was used for the CG model of C$_{60}$. Figure 3 illustrates the coarse-graining scheme used.

The interactions between CG sites were iteratively optimized to reproduce the atomistic system's structure (radial distribution functions (RDFs) of nonbonded sites and bond, angle, and dihedral distributions) using the iterative Boltzmann inversion (IBI) method, which has been described elsewhere in detail.[41,42] In our implementation of the IBI method, the potential energy $U_{i+1}(x)$ of a particular interaction type at the $(i + 1)$th iteration was calculated from the potential energy $U_i(x)$ at the ith iteration using

$$U_{i+1}(x) = U_i(x) + a_i k_{\mathrm{B}} T \ln\left[\frac{P_i(x)}{P^{\mathrm{target}}(x)}\right] \quad (1)$$

where $P_i(x)$ is the probability distribution of the variable x calculated from the CG simulation during iteration i, $P^{\mathrm{target}}(x)$ is the target distribution calculated from the atomistic simulation (x can be the distance r, bond length l, bond angle θ, proper dihedral angle ϕ, or improper dihedral angle ξ for nonbonded interactions, bond stretching, bond bending, or proper or improper torsions, respectively), and $0 \leq a_i \leq 1$ (a_i was decreased or increased between iterations depending on whether the CG probability distribution diverged from or converged too slowly to the target distribution in the preceding iteration). For the initial potential energy function, we used

$$U_0(x) = -k_{\mathrm{B}} T \ln[P^{\mathrm{target}}(x)] \quad (2)$$

where $P_{\mathrm{target}}(x) \propto g_{\mathrm{target}}(r)$ (the RDF), $P_{\mathrm{bond}}^{\mathrm{target}}(l)/l^2$, $P_{\mathrm{angle}}^{\mathrm{target}}(\theta)/\sin\theta$, $P_{\mathrm{dihed}}^{\mathrm{target}}(\phi)$, and $P_{\mathrm{improp}}^{\mathrm{target}}(\xi)$, respectively, for nonbonded interactions, bond stretching, bond bending, and proper and improper torsions.

The CG simulations in which the CG interactions were optimized were carried out at constant temperature (NVT ensemble) with a Nosé–Hoover thermostat.[50] After optimization of the interactions using the above procedure, a linear correction,[41]

$$\Delta U_{jk}(r) = b_{jk}\left(1 - \frac{r}{r_{\mathrm{c}}}\right), \quad r \leq r_{\mathrm{c}} \quad (3)$$

was added to all nonbonded interactions so that the pressure of the CG simulations matched those of the atomistic simulations (1 atm in all cases) and so that the RDFs were unchanged from the Boltzmann inversion step. Here r_{c} is the cutoff distance in the nonbonded CG interactions ($r_{\mathrm{c}} = 20$, 25, and 27 Å, respectively, for the P3HT–P3HT, P3HT–C$_{60}$, and C$_{60}$–C$_{60}$ interactions) and b_{jk} is a constant for each pair of site types j and k ($b_{jk} = -0.282$, -0.158, and -2.063 kcal/mol, respectively, for the P3HT–P3HT, P3HT–C$_{60}$, and C$_{60}$–C$_{60}$ interactions).

The P3HT–P3HT CG interactions were optimized in simulations of pure P3HT (60 3HT 12-mers) at 550 K. Then, the P3HT–C$_{60}$ and C$_{60}$–C$_{60}$ CG interactions were optimized in simulations of 1.85:1 w/w P3HT:C$_{60}$ (48 3HT12 and 72 C$_{60}$) at 550 K with the P3HT–P3HT CG interactions fixed at their previously optimized values. Optimization of the CG interactions was carried out at 550 K to ensure that the systems were in the fluid state, because the use of isotropic interaction potentials between nonbonded pairs of sites implicitly assumes that the nonbonded site–site distributions in the atomistic systems from which the CG interactions are derived are isotropic as well. The use of isotropic nonbonded pair potentials in the CG models does not, however, preclude phase separation of the CG system as the temperature or mixture composition is varied, because phase separation arises from the collective interactions of many particles, nor does it mean that the CG models will not reasonably capture the behavior of the system as phase separation occurs. The CG nonbonded interaction potentials were defined numeri-
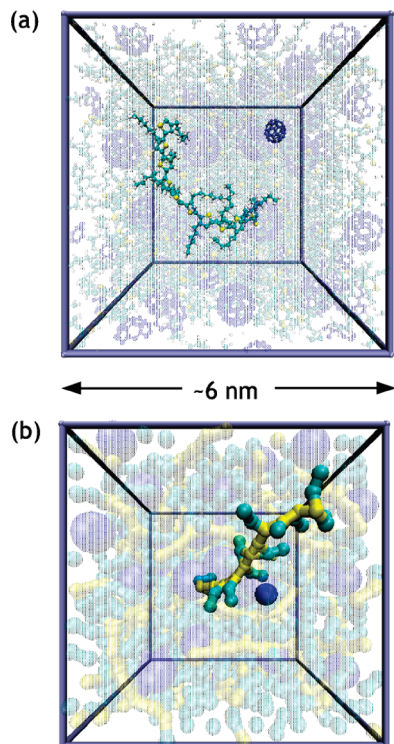
Polymer/Fullerene Bulk Heterojunctions

J. Chem. Theory Comput., Vol. 6, No. 2, 2010 **531**

Figure 4. Snapshots of configurations from (a) atomistic and (b) coarse-grained simulations of 48 3HT 12-mers and 72 C_{60} molecules (P3HT:C_{60} = 1.85:1 w/w) at 550 K and 1 atm. A single molecule of each type is highlighted.

Figure 5. Radial distribution functions $g(r)$ for nonbonded sites computed from constant NPT atomistic simulations of 60 P3HT 12-mers at 550 K and 1 atm (solid lines) and from constant NVT CG simulations at 550 K with optimized CG interaction potentials (dotted lines, which are almost indistinguishable from the solid lines). The optimized CG potentials $U_{nb}(r)$ are given by the dashed lines. (See Figure 3 for definitions of site types.)

cally at grid points, while the CG bonded interaction potentials were fit to polynomials in l, θ, cos (ϕ), and ξ, respectively, for bonds, angles, proper dihedrals, and improper dihedrals (see the Supporting Information for the model parameters). The end monomers of the oligomer chains were excluded from the calculation of distribution functions used in the optimization procedure to reduce end effects. A time-step of 5 fs was used in the CG simulations. Figure 4 shows typical snapshots from atomistic and CG simulations of mixtures of 3HT 12-mers and C_{60}.

4. Optimized Coarse-Grained Potentials

Approximately 10 Boltzmann inversion iterations each were required to optimize the CG interaction potentials for the pure 3HT12 system and for the 3HT12/C_{60} mixture. Figures 5−9 depict, respectively, the radial distribution functions and bond length, bond angle, proper dihedral angle, and improper dihedral angle probability distributions for the pure 3HT12 system at 550 K from the atomistic simulation and from the CG simulation with the optimized CG interactions. The corresponding optimized CG interaction potentials are also shown. A few representative joint bond-length/bond-angle and bond-angle/dihedral-angle probability distributions from the atomistic and CG simulations are also plotted in the Supporting Information and show that the coarse-grained model accurately reproduces the cross-correlations between the bonded degrees of freedom in P3HT (the agreement between the joint probability distributions that are not shown is similarly good).
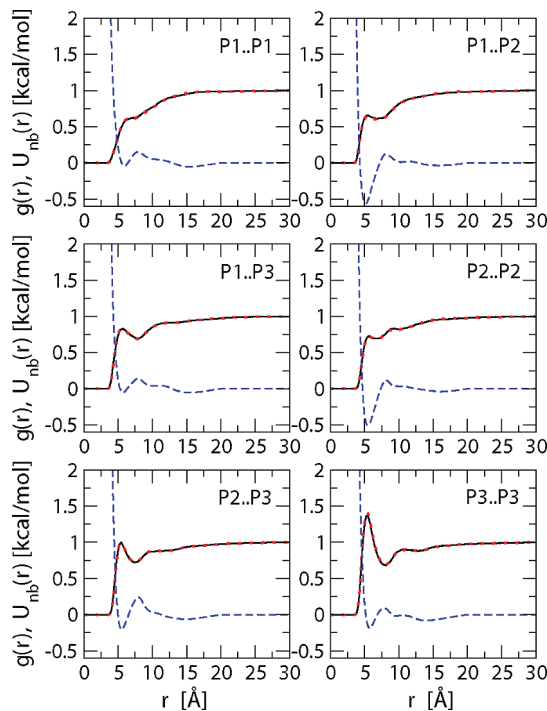
Figure 6 and Figure 7 show that the bond length and angle distributions are unimodal and for the most part quite sharp, indicating that the bonds and angles in the CG model of P3HT are well-defined and physically meaningful. Note that because our rr-P3HT chains have directionality to them (much like a polypeptide has an N and a C terminus), distributions for the P1−P1−P2 and P2−P1−P1 angles and P1−P1−P2−P3 and P3−P2−P1−P1 proper dihedrals are different.

Figure 8 shows that the P2−P1−P1−P2 dihedral angle is roughly twice as likely to be 180° than to be 0°, indicating that on average every third monomer is in the syn conformation relative to one of its neighbors at 550 K. The higher probability of a P1−P1−P1−P1 dihedral angle of 0° compared with one of 180° shown in Figure 8 is consistent with configurations in which four monomers in a row are in the anti conformation being less common than those in which one pair is in the syn conformation. These findings are consistent with IR spectroscopic measurements on rr-P3HT thin films of the antisymmetric side-chain methylene stretch, which is sensitive to the chain conformation, which show a frequency more characteristic of a disordered chain than an all-anti conformation.[30] Other measurements also indicate that the conformation of P3HT chains, and rr-P3HT in particular, is not highly ordered: the vibrational frequency of the antisymmetric carbon−carbon stretch of the polymer backbone in rr-P3HT thin films indicate a conjugation length of five or six monomer units,[30,62] and although not strictly comparable with results on pure rr-P3HT films or melts, a
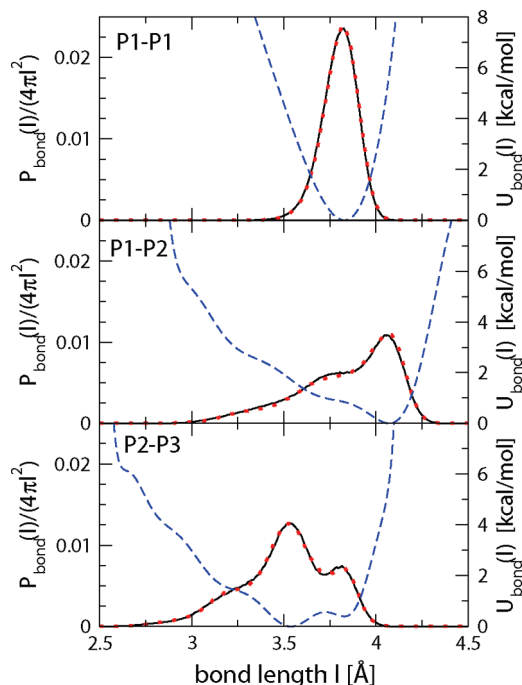
Figure 6. Bond length probability distributions $P_{bond}(l)$ computed from constant NPT atomistic simulations of 60 P3HT 12-mers at 550 K and 1 atm (solid lines) and from constant NVT CG simulations at 550 K (dotted lines) with optimized CG interaction potentials. The optimized CG bond ptentials $U_{bond}(l)$ are given by the dashed lines. (See Figure 3 for definitions of site types.)
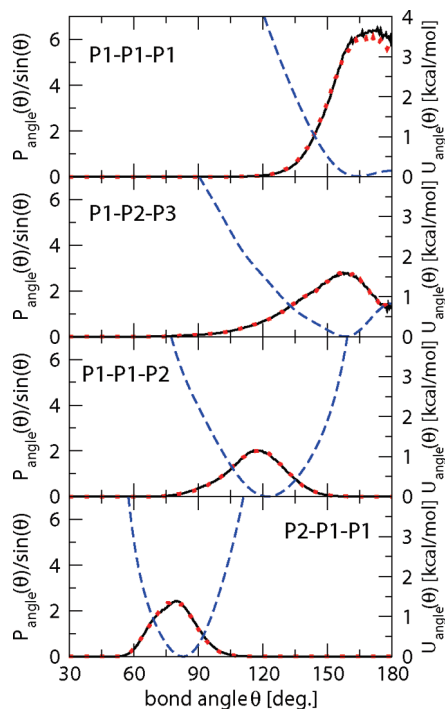

Figure 7. Bond angle probability distributions $P_{angle}(\theta)$ computed from constant NPT atomistic simulations of 60 P3HT 12-mers at 550 K and 1 atm (solid lines) and from constant NVT CG simulations at 550 K (dotted lines) with optimized CG interaction potentials. The optimized CG bond angle potentials $U_{angle}(\theta)$ are given by the dashed lines. (See Figure 3 for definitions of site types.)
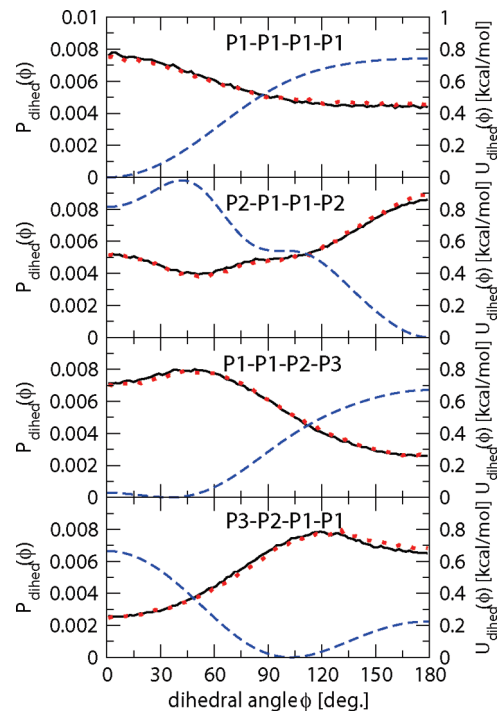

Figure 8. Dihedral angle probability distributions $P_{dihed}(\phi)$ computed from constant NPT atomistic simulations of 60 P3HT 12-mers at 550 K and 1 atm (solid lines) and from constant NVT CG simulations at 550 K (dotted lines) with optimized CG interaction potentials. The optimized CG dihedral potentials $U_{dihed}(\phi)$ are given by the dashed lines. (See Figure 3 for definitions of site types.)

persistence length of 2.4 ± 0.3 nm or roughly six monomer units has been measured for P3HT in THF at room temperature by light scattering.[63] These results indicate that P3HT does not exist in the completely ordered all-anti conformation, as is often depicted,[15,23,64] but is only ordered for roughly six monomer units on average. This value of five or six units (i.e., a 1:5 or 1:6 ratio of syn and anti conformers) measured experimentally at room temperature is consistent with a Boltzmann distribution of conformers with the same intermonomer torsion potential (the points in Figure 2) as that used in our simulation model, indicating that the torsion potential in our model provides an accurate description of the P3HT intermonomer dihedral. At the higher temperature of 550 K used in the simulations, this intermonomer torsion potential leads to the smaller 1:2 ratio of syn to anti conformers observed in Figure 8. The available X-ray diffraction data, while supporting the picture of the all-anti herringbone conformation of P3HT,[15,23,64] does not rule out the possibility of the occasional monomer pair existing in the syn conformation. This is a point worthy of further experimental study; our simulation model, which uses an intermonomer torsion potential from ab initio quantum calculations and which is consistent with several experimental results as discussed above, supports the picture of rr-P3HT existing mostly in the anti conformation but with a significant proportion of monomer pairs having a syn conformation.

Turning to the P3HT–C$_{60}$ and C$_{60}$–C$_{60}$ interactions, Figure 10 depicts the radial distribution functions from the 1.85:1

Polymer/Fullerene Bulk Heterojunctions
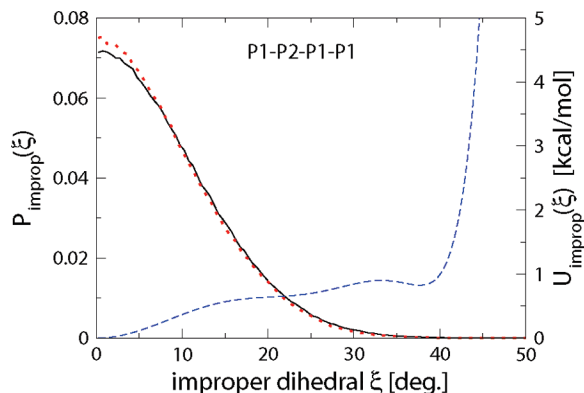
J. Chem. Theory Comput., Vol. 6, No. 2, 2010 **533**

Figure 9. P1−P2−P1−P1 improper dihedral angle probability distribution $P_{improp}(\xi)$ (see Figure 3 for definitions of site types) computed from constant NPT atomistic simulations of 60 P3HT 12-mers at 550 K and 1 atm (solid line) and constant NVT CG simulations at 550 K (dotted line) with optimized CG interaction potentials. The optimized CG improper dihedral potential $U_{improp}(\xi)$ is given by the dashed line.
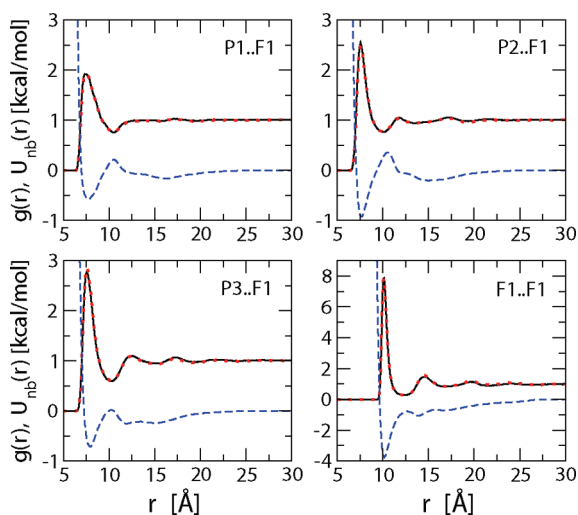

Figure 10. Radial distribution functions $g(r)$ for nonbonded sites computed from constant NPT atomistic simulations of 48 P3HT 12-mers and 72 C_{60} molecules at 550 K and 1 atm (solid lines) and constant NVT CG simulations with optimized CG interaction potentials at 550 K (dotted lines, which are almost indistinguishable from the solid lines). The optimized CG nonbonded interaction potentials $U_{nb}(r)$ are given by the dashed lines. (See Figure 3 for definitions of site types.)

w/w mixture of P3HT 12-mers and C_{60} at 550 K from the constant NPT atomistic simulation and from the constant NVT CG simulation with optimized CG interaction potentials. The corresponding optimized CG interaction potentials are also shown. Similarly good agreement between the atomistic and CG simulations to that shown in Figure 5 was found for the P3HT−P3HT distributions (not shown), even though the P3HT−P3HT interactions were not optimized in these simulations of P3HT/C_{60} mixtures.

5. State-Point Dependence

In order to be generally useful, the CG models should accurately describe the behavior of the system at different thermodynamic states from those at which they were
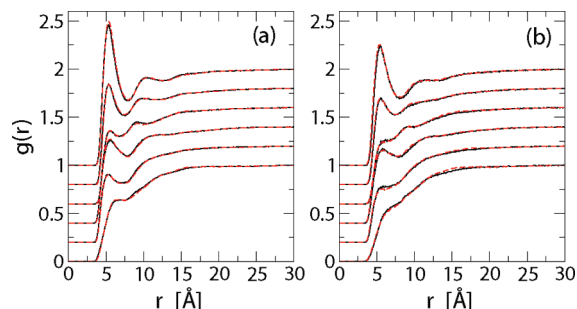

Figure 11. Radial distribution functions (RDFs) for non-bonded sites from constant NPT atomistic (solid lines) and CG simulations (dashed lines, which are almost indistinguishable from the solid lines) of 60 P3HT 12-mers at (a) 500 and (b) 650 K. (RDFs have been shifted vertically for ease of viewing; site pairs (from bottom to top): P1..P1, P1..P2, P1..P3, P2..P2, P2..P3, and P3..P3 (see Figure 3 for definitions of site types).)
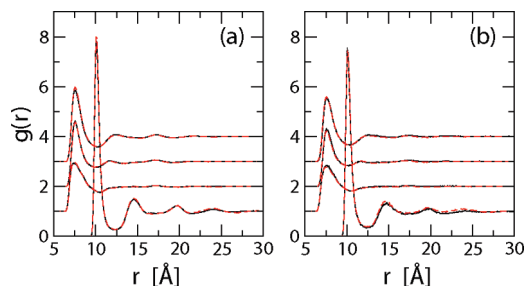

Figure 12. Radial distribution functions (RDFs) for polymer−fullerene and fullerene−fullerene site pairs from constant NPT atomistic (solid lines) and CG simulations (dashed lines, which are almost indistinguishable from solid lines) for 3HT12:C_{60} (w/w) of (a) 1.27:1 at 550 K and (b) 1.85:1 at 650 K. (RDFs have been shifted vertically for ease of viewing; site pairs (from bottom to top): P1..F1, P2..F1, P3..F1, and F1..F1 (see Figure 3 for definitions of site types).)

parametrized. We have therefore carried out constant NPT CG simulations at 1 atm of 3HT12/C_{60} mixtures at temperatures other than 550 K and for P3HT:C_{60} mixture ratios other than 1:0 and 1.85:1 w/w and have compared the resulting distributions with those of equivalent atomistic simulations. Figure 11 shows the RDFs for nonbonded sites from constant NPT atomistic and CG simulations of pure P3HT at 500 and 650 K at 1 atm. There is perfect agreement between the CG and atomistic simulations at both temperatures. The agreement between the atomistic and CG simulations for the bonded distributions (bond lengths, angles, and dihedrals), although not shown, is equally good.

Figure 12 shows the RDFs for P3HT−C_{60} and C_{60}−C_{60} site pairs for 3HT12/C_{60} mixtures at a couple of different temperatures and mixture compositions at 1 atm. For the systems presented in Figure 12 and also for all of the other thermodynamic states studied, all of the CG distributions agree with the atomistic ones, within the error bars on the points. (The P3HT−P3HT distributions are not shown for the P3HT/C_{60} mixtures but display similarly good agreement.) The pure P3HT system at 500 K and the P3HT:C_{60} = 1.27:1 w/w system at 550 K, in particular, are likely to be at or close to phase coexistence, given the experimental phase diagrams of P3HT:PCBM mixtures[31,32] and the highly
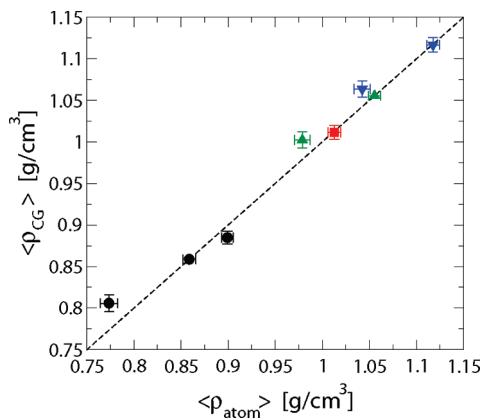
Figure 13. Average total density $\langle \rho_{CG} \rangle$ from constant NPT CG simulations vs average total density $\langle \rho_{atom} \rangle$ from constant NPT atomistic simulations for the same mixture composition and temperature (3HT12:C_{60} (w/w) = 1:0 (circles), 2.52:1 (squares), 1.85:1 (up triangles), and 1.27:1 (down triangles)).

structured $C_{60}-C_{60}$ RDF for the P3HT/C_{60} mixture: the close agreement between the RDFs from the atomistic and CG simulations indicates that the CG models can reasonably describe the phase separation of these mixtures.

The results of all of our comparisons between the atomistic and CG simulations at different state points are summarized in Figure 13 in terms of the average total density $\langle \rho_{CG} \rangle$ measured in the CG simulations as a function of the average total density $\langle \rho_{atom} \rangle$ in the corresponding atomistic simulations. The line $\langle \rho_{CG} \rangle = \langle \rho_{atom} \rangle$ is also shown to indicate how closely the CG and atomistic densities agree with each other. It can be seen that the agreement is good, particularly at 500 and 550 K. The largest discrepancy between the densities of the CG and atomistic systems occurs for the pure P3HT system at 650 K, at which the CG system is $4 \pm 2\%$ more dense than the atomistic system. This difference is actually quite small for CG simulations models.[61,65,66] A 650 K temperature is also much higher than the temperatures that are typically used in processing polymer solar cells; the small discrepancy at this temperature shows that our CG models perform reasonably well even at thermodynamic conditions well outside those at which it is likely to be used.

6. Atomistic vs Coarse-Grained Time Scales

The CG interaction potentials that we have constructed for P3HT/C_{60} mixtures have been optimized for the fluid structure (see section 3) and not for the dynamics. Therefore, it can be expected that the time scales for dynamics in the CG simulations will not be equivalent to those in the atomistic simulations.[39,67] No theory currently exists for predicting the time scales of a CG simulation relative to those of the atomistic simulation from which it was derived. Development of such a theory is beyond the scope of this work, but an estimate of the relative time scales of the atomistic and CG simulations is useful for comparing the CG simulation dynamics with experimental data.

We have estimated the relative time scales by comparing transport coefficients calculated from simulations of the atomistic and CG systems: translational time scales were
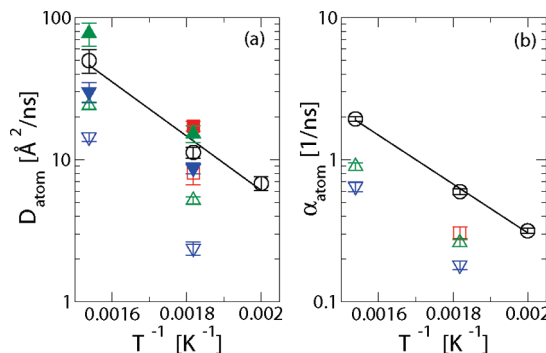

Figure 14. (a) Translational diffusion coefficient D_{atom} for 3HT12 monomers (empty symbols) and C_{60} (filled symbols) and (b) rotational diffusion coefficient α_{atom} for 3HT12 chains from atomistic simulations as a function of $1/T$ for various 3HT12:C_{60} weight ratios: 1:0 (circles), 2.52:1 (squares), 1.85:1 (triangles up), and 1.27:1 (triangles down). The lines are exponential (Arrhenius) fits to the circles.

determined by calculating the mean squared displacement (MSD) $\langle r^2(t) \rangle$ of the monomer center-of-mass in the P3HT chains (using only the central four monomers in each chain for the calculation) and of the C_{60} center-of-mass; rotational time scales were obtained by calculating the orientational correlation function $\langle P_2[\hat{\mathbf{u}}(t) \cdot \hat{\mathbf{u}}(0)] \rangle \equiv \langle P_2[\cos \Theta(t)] \rangle$ of the unit vector $\hat{\mathbf{u}}$ connecting the polymer chain ends (defined by the centers-of-mass of the end thiophene rings). For diffusive translational motion,

$$\langle r^2(t) \rangle \sim 6Dt \tag{4}$$

and for diffusive rotational motion,

$$\langle P_2[\cos \Theta(t)] \rangle \sim \exp(-\alpha t) \tag{5}$$

where D and α are the translational and rotational diffusion coefficients, respectively. For all of the simulations, we found, after an initial transient time, that $\langle r^2(t) \rangle$ and $\langle P_2[\cos \Theta(t)] \rangle$ were well fit by eqs 4 and 5, respectively, allowing well-defined values of D and α to be extracted. The ratios D_{CG}/D_{atom} and $\alpha_{CG}/\alpha_{atom}$, where the subscripts "atom" and "CG" denote quantities measured in the atomistic and CG simulations respectively, provide estimates of the relative time scales of the CG simulations compared with the atomistic simulations (the relative translational and rotational time scales defined by D_{CG}/D_{atom} and $\alpha_{CG}/\alpha_{atom}$ are not necessarily the same but are expected to be comparable).

Before comparison of the atomistic and CG time scales, we first present in Figure 14 the translational and rotational diffusion coefficients measured in the atomistic simulations as functions of the temperature and the P3HT:C_{60} mixture ratio. As expected, D and α increase with T, with an approximately exponential dependence on $1/T$ that is indicative of activated diffusion. The activation energies for translational and rotational motion (given by the slope of the lines between the points of the same mixture composition) are comparable, although not equal. D and α also decrease monotonically with increasing C_{60} concentration. This is not surprising, given that the sublimation point of C_{60}[68] is substantially higher than the melting point of pure P3HT,[31] and so the addition of increasing amounts of C_{60} appears to

Polymer/Fullerene Bulk Heterojunctions

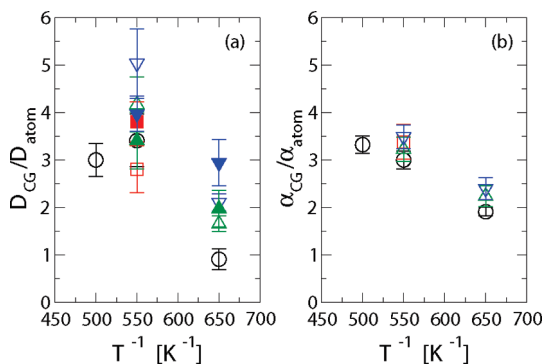*J. Chem. Theory Comput., Vol. 6, No. 2, 2010* **535**

Figure 15. (a) Ratio of translational diffusion coefficients, D_{CG}/D_{atom}, for 3HT12 monomers (empty symbols) and C_{60} (filled symbols) and (b) ratio of rotational diffusion coefficients, $\alpha_{CG}/\alpha_{atom}$, from CG and atomistic simulations as a function of temperature for various 3HT12:C_{60} weight ratios: 1:0 (circles), 2.52:1 (squares), 1.85:1 (triangles up), and 1.27:1 (triangles down).

move the systems closer to the freezing point of the mixture. We do not see evidence of a freezing point depression at intermediate fullerene concentrations that has been observed experimentally for P3HT:PCBM mixtures, which have a eutectic point for 65% P3HT (2:1 w/w P3HT:PCBM).[31] PCBM, however, mixes more readily with P3HT than does C_{60} and is expected to have a lower melting/sublimation point due to the disordering effect of its side chain.

Turning to the relative time scales for the atomistic and CG simulations, D_{CG}/D_{atom} and $\alpha_{CG}/\alpha_{atom}$ are plotted as a function of temperature in Figure 15 for the various P3HT:C_{60} mixture ratios studied. It can be seen that, in almost all cases, the translational and rotational time scales are larger for the CG simulations than for the atomistic simulations The relative time scales are also fairly insensitive to mixture composition; the data suggests that they may increase with increasing C_{60} content, but the large error bars on the points (particularly for the 3HT12 monomer translational diffusion coefficient) make it difficult to verify this hypothesis conclusively. The relative time scales also decrease with increasing temperature in almost all cases. The latter result is consistent with the expectation that the dynamics in the CG simulations occurs on a less rugged potential energy landscape with lower peaks and shallower valleys. The relative translational time scale for the pure P3HT system at 650 K does not follow the expected trend, possibly because of the higher average density in the CG simulation compared with the atomistic simulation (see section 5). The relative rotational time scale for pure P3HT at this temperature, however, displays the expected behavior: rotational motion of the polymer chains is not expected to be as sensitive to the density as translational motion, because in order to diffuse a polymer always needs to change place with its neighbors whereas reorientation can partially be achieved without displacement of other chains.

Taking into account the 2- to 5-fold difference between the CG and atomistic time scales and the 3-fold larger time step used in the CG simulations compared with the atomistic simulations, and the 10-fold speed-up in the simulation at each time-step for the systems studied, an overall speed-up

of over 2 orders of magnitude is obtained in the CG simulations. This result underscores the huge advantage of the CG simulations over atomistic ones, particularly for large systems.

7. Device-Scale Molecular Simulations of Bulk Heterojunctions

Our CG model makes possible the study of the structure and dynamic evolution of the bulk heterojunction (BHJ) microstructure in systems approaching the device scale, because of the substantial speed-up over atomistic simulations discussed in section 6. As a proof-of-principle of the feasibility of studying device-scale bulk heterojunctions with our CG models, we have carried out a simulation of 768 P3HT 48-mers (MW $\sim$ 8 kDa) and 4608 C_{60} molecules (1.85:1 w/w P3HT:C_{60}) in which the system, initially consisting of randomly placed polymer chains and fullerenes, was cooled over a period of 10 ns (CG time scale) from 550 to 490 K, after equilibrating at 550 K for 1 ns. The molecular weight of the polymer chains of 8 kDa is close to the ideal molecular weight for P3HT:fullerene solar cells of 13−34 kDa.[69] The average simulation box size length is roughly 25 nm, of the same order as the 50−100 nm[70,71] typically used for the thickness of the active layer in polymer solar cells. The simulation took approximately 24 h on 256 2.3-GHz AMD Opteron processors.

Figure 16 depicts snapshots of the system as a function of time as the system is cooled, in which P3HT and C_{60} appear to begin to phase separate as time progresses. In this initial test of our CG models in a device-scale simulation, the cooling of the system has been carried out very rapidly (the total length of the simulation is shorter than the chain reorientational time scale τ_2), and so the system is likely in a nonequilibrium state throughout the simulation. It is expected that phase separation would be even more evident if the cooling were carried out at a slower rate. Simulations at least 1 order of magnitude longer are feasible with our CG models for systems of this size and are in the process of being carried out.

It should be noted that the way in which the polymer/fullerene system was evolved in this simulation is not the same as the way in which polymer/fullerene solar cells are normally fabricated, in that the active layer in the latter case is deposited from a solvent. Rather, these simulations can describe the annealing step that is usually used in fabrication to improve device performance,[10,12] in which the solar cell is heated above its glass transition temperature to "improve" the BHJ morphology. CG simulation of polymer/fullerene mixtures in solution are, however, possible and represent a potential future step of this work.

8. Conclusions

In summary, we have developed coarse-grained (CG) computer simulation models of P3HT and P3HT/C_{60} mixtures and verified that the models accurately describe the structure of these materials over a range of thermodynamic conditions other than those at which the CG models were parametrized. We have also demonstrated in a preliminary study of phase
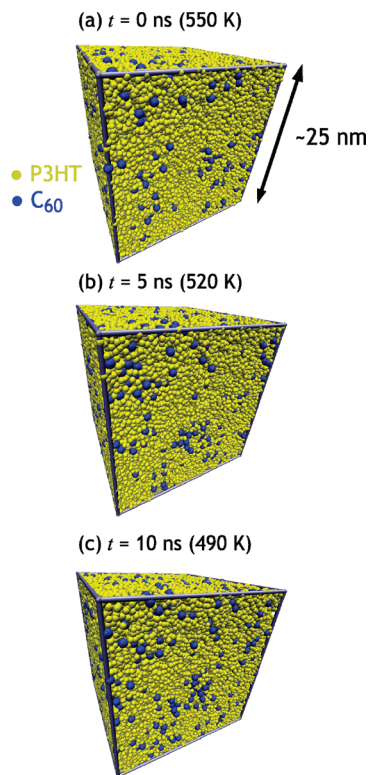
536 *J. Chem. Theory Comput., Vol. 6, No. 2, 2010*

Huang et al.

(a) *t* = 0 ns (550 K)

● P3HT
● C$_{60}$

~25 nm

(b) *t* = 5 ns (520 K)

(c) *t* = 10 ns (490 K)

Figure 16. Snapshots from a constant NPT CG simulation of 768 P3HT 48-mers (MW ~8 kDa) and 4608 C$_{60}$ molecules (1.85:1 w/w P3HT:C$_{60}$, 115 200 particles) in which the system is cooled from 550 to 490 K over a period of 10 ns (the system is periodically replicated in all three directions). The initial configuration consisted of randomly placed chains and fullerenes. P3HT and C$_{60}$ particles are in yellow and blue, respectively.

separation of a P3HT/C$_{60}$ mixture that the CG models can be used to study the structure and dynamic evolution of bulk heterojunctions at the molecular level for systems approaching the scale of organic photovoltaic devices.

In a subsequent publication, we will analyze in quantitative detail the structure and dynamic evolution of the BHJ microstructure (e.g., crystallinity, domain size, domain connectivity, chain persistence length, etc.) in these device-scale CG simulations as functions of the polymer:fullerene mole fraction and polymer chain length. We are also parametrizing a CG model of PCBM, the most widely used electron acceptor in polymer-based solar cells, having demonstrated the feasibility of CG simulations for C$_{60}$. In future work, we plan to study other polymer and fullerene types and to include solvent molecules in the CG simulations, thereby more closely mimicking the experimental processes by which BHJs are formed in organic solar cells.

Supporting Information Available: Atomistic and coarse-grained simulation model parameters for P3HT and C$_{60}$ and selected joint bond-length/bond-angle and bond-angle/dihedral-angle probability distributions from the atomistic and coarse-grained simulations. This information is available free of charge via the Internet at http://pubs.acs.org.

References

(1) U.S. Department of Energy, *Basic Research Needs for Solar Energy Utilization*, 2005.

(2) U.S. Department of Energy, *New Science for a Secure and Sustainable Energy Future*, 2008.

(3) Lewis, N. S. *MRS Bull.* **2007**, *32*, 808–820.

(4) Lewis, N. S. *Science* **2007**, *315*, 798–801.

(5) Brabec, C. J.; Hauch, J. A.; Schilinsky, P.; Waldauf, C. *MRS Bull.* **2005**, *30*, 50–52.

(6) Markov, D. E.; Amsterdam, E.; Blom, P. W. M.; Sieval, A. B.; Hummelen, J. C. *J. Phys. Chem. A* **2005**, *109*, 5266–5274.

(7) Mayer, A. C.; Scully, S. R.; Hardin, B. E.; Rowell, M. W.; McGehee, M. D. *Mater. Today* **2007**, *10*, 28–33.

(8) Coropceanu, V.; Cornil, J.; da Silva, D. A.; Olivier, Y.; Silbey, R.; Brédas, J. L. *Chem. Rev.* **2007**, *107*, 926–952.

(9) Schilinsky, P.; Asawapirom, U.; Scherf, U.; Biele, M.; Brabec, C. J. *Chem. Mater.* **2005**, *17*, 2175–2180.

(10) Padinger, F.; Rittberger, R. S.; Sariciftci, N. S. *Adv. Funct. Mater.* **2003**, *13*, 85–88.

(11) Li, G.; Shrotriya, V.; Huang, J.; Yao, Y.; Moriarty, T.; Emery, K.; Yang, Y. *Nat. Mater.* **2005**, *4*, 864–868.

(12) Ma, W.; Yang, C.; Gong, X.; Lee, K.; Heeger, A. J. *Adv. Funct. Mater.* **2005**, *15*, 1617–1622.

(13) Saunders, B. R.; Turner, M. L. *Adv. Colloid Interface Sci.* **2008**, *138*, 1–23.

(14) Chabinyc, M. L. *Polymer Rev.* **2008**, *48*, 463–492.

(15) Chen, T. A.; Wu, X. M.; Rieke, R. D. *J. Am. Chem. Soc.* **1995**, *117*, 233–244.

(16) Prosa, T. J.; Winokur, M. J.; Moulton, J.; Smith, P.; Heeger, A. J. *Macromolecules* **1992**, *25*, 4364–4372.

(17) Yang, C.; Orfino, F. P.; Holdcroft, S. *Macromolecules* **1996**, *29*, 6510–6517.

(18) Sirringhaus, H.; Brown, P. J.; Friend, R. H.; Nielsen, M. M.; Bechgaard, K.; Langeveld-Voss, B. M. W.; Spiering, A. J. H.; Janssen, R. A. J.; Meijer, E. W.; Herwig, P.; de Leeuw, D. M. *Nature* **1999**, *401*, 685–688.

(19) Aasmundtveit, K. E.; Samuelsen, E. J.; Guldstein, M.; Steinsland, C.; Flornes, O.; Fagermo, C.; Seeberg, T. M.; Pettersson, L. A. A.; Inganäs, O.; Feidenhans'l, R.; Ferrer, S. *Macromolecules* **2000**, *33*, 3120–3127.

(20) Hugger, S.; Thomann, R.; Heinzel, T.; Thurn-Albrecht, T. *Colloid Polym. Sci.* **2004**, *282*, 932–938.

(21) Kline, R. J.; McGehee, M. D.; Kadnikova, E. N.; Liu, J. S.; Fréchet, J. M. J.; Toney, M. F. *Macromolecules* **2005**, *38*, 3312–3319.

(22) Erb, T.; Zhokhavets, U.; Gobsch, G.; Raleva, S.; Stuhn, B.; Schilinsky, P.; Waldauf, C.; Brabec, C. J. *Adv. Funct. Mater.* **2005**, *15*, 1193–1196.

(23) Kim, Y.; Cook, S.; Tuladhar, S. M.; Choulis, S. A.; Nelson, J.; Durrant, J. R.; Bradley, D. D. C.; Giles, M.; McCulloch, I.; Ha, C. S.; Ree, M. *Nat. Mater.* **2006**, *5*, 197–203.

Polymer/Fullerene Bulk Heterojunctions

J. Chem. Theory Comput., Vol. 6, No. 2, 2010 **537**

(24) Chang, J. F.; Clark, J.; Zhao, N.; Sirringhaus, H.; Breiby, D. W.; Andreasen, J. W.; Nielsen, M. M.; Giles, M.; Heeney, M.; McCulloch, I. *Phys. Rev. B* **2006**, *74*, 115318.

(25) Zen, A.; Saphiannikova, M.; Neher, D.; Grenzer, J.; Grigorian, S.; Pietsch, U.; Asawapirom, U.; Janietz, S.; Scherf, U.; Lieberwirth, I.; Wegner, G. *Macromolecules* **2006**, *39*, 2162–2171.

(26) Kline, R. J.; DeLongchamp, D. M.; Fischer, D. A.; Lin, E. K.; Richter, L. J.; Chabinyc, M. L.; Toney, M. F.; Heeney, M.; McCulloch, I. *Macromolecules* **2007**, *40*, 7960–7965.

(27) Zhang, R.; Li, B.; Iovu, M. C.; Jeffries-EL, M.; Sauve, G.; Cooper, J.; Jia, S. J.; Tristram-Nagle, S.; Smilgies, D. M.; Lambeth, D. N.; McCullough, R. D.; Kowalewski, T. *J. Am. Chem. Soc.* **2006**, *128*, 3480–3481.

(28) Andersson, B. V.; Herland, A.; Masich, S.; Inganäs, O. *Nano Lett.* **2009**, *9*, 853–855.

(29) van Bavel, S. S.; Sourty, E.; de With, G.; Loos, J. *Nano Lett.* **2009**, *9*, 507–513.

(30) Gurau, M. C.; Delongchamp, D. M.; Vogel, B. M.; Lin, E. K.; Fischer, D. A.; Sambasivan, S.; Richter, L. J. *Langmuir* **2007**, *23*, 834–842.

(31) Müller, C.; Ferenczi, T. A. M.; Campoy-Quiles, M.; Frost, J. M.; Bradley, D. D. C.; Smith, P.; Stingelin-Stutzmann, N.; Nelson, J. *Adv. Mater.* **2008**, *20*, 3510–3515.

(32) Kim, J. Y.; Frisbie, C. D. *J. Phys. Chem. C* **2008**, *112*, 17726–17736.

(33) Cheung, D. L.; Troisi, A. *Phys. Chem. Chem. Phys.* **2008**, *10*, 5941–5952.

(34) Corish, J.; Feeley, D. E.; Morton-Blake, D. A.; Béniere, F.; Marchetti, M. *J. Phys. Chem. B* **1997**, *101*, 10075–10085.

(35) Curco, D.; Aleman, C. *J. Comput. Chem.* **2007**, *28*, 1743–1749.

(36) Kirkpatrick, J.; Marcon, V.; Nelson, J.; Kremer, K.; Andrienko, D. *Phys. Rev. Lett.* **2007**, *98*, 227402.

(37) Troisi, A.; Cheung, D. L.; Andrienko, D. *Phys. Rev. Lett.* **2009**, *102*, 116602.

(38) Coropceanu, V.; Sanchez-Carrera, R. S.; Paramonov, P.; Day, G. M.; Brédas, J. L. *J. Phys. Chem. C* **2009**, *113*, 4679–4686.

(39) Tschöp, W.; Kremer, K.; Batoulis, J.; Bürger, T.; Hahn, O. *Acta Polym.* **1998**, *49*, 61–74.

(40) Baschnagel, J.; Binder, K.; Doruker, P.; Gusev, A. A.; Hahn, O.; Kremer, K.; Mattice, W. L.; Müller-Plathe, F.; Murat, M.; Paul, W.; Santos, S.; Suter, U. W.; Tries, V. *Adv. Polym. Sci.* **2000**, *152*, 41–156.

(41) Reith, D.; Pütz, M.; Müller-Plathe, F. *J. Comput. Chem.* **2003**, *24*, 1624–1636.

(42) Faller, R.; Reith, D. *Macromolecules* **2003**, *36*, 5406–5414.

(43) *Coarse-Graining of Condensed Phase and Biomolecular Systems*; Voth, G. A., Ed.; CRC Press: Boca Raton, FL, 2008.

(44) Marcon, V.; Raos, G. *J. Am. Chem. Soc.* **2006**, *128*, 1408–1409.

(45) Marcon, V.; Raos, G. *J. Phys. Chem. B* **2004**, *108*, 18053–18064.

(46) Jorgensen, W. L.; Maxwell, D. S.; Tirado-Rives, J. *J. Am. Chem. Soc.* **1996**, *118*, 11225–11236.

(47) Plimpton, S. J. *J. Comput. Phys.* **1995**, *117*, 1–19; LAMMPS Molecular Dynamics Simulator: http://lammps.sandia.gov.

(48) Hockney, R. W.; Eastwood, J. W. *Computer Simulation Using Particles*; Institute of Physics Publishing, Bristol, 1988.

(49) Ryckaert, J. P.; Ciccotti, G.; Berendsen, H. J. C. *J. Comput. Phys.* **1977**, *23*, 327–341.

(50) Hoover, W. G. *Phys. Rev. A* **1985**, *31*, 1695–1697.

(51) Hoover, W. G. *Phys. Rev. A* **1986**, *34*, 2499–2500.

(52) Raos, G.; Famulari, A.; Marcon, V. *Chem. Phys. Lett.* **2003**, *379*, 364–372.

(53) Darling, S. B.; Sternberg, M. *J. Phys. Chem. B* **2009**, *113*, 6215–6218.

(54) Barbarella, G.; Zambianchi, M.; Bongini, A.; Antolini, L. *Adv. Mater.* **1994**, *6*, 561–564.

(55) Price, M. L. P.; Ostrovsky, D.; Jorgensen, W. L. *J. Comput. Chem.* **2001**, *22*, 1340–1352.

(56) Sigma-Aldrich Catalog: http://www.sigmaaldrich.com.

(57) Mardalen, J.; Samuelsen, E. J.; Gautun, O. R.; Carlsen, P. H. *Solid State Commun.* **1991**, *77*, 337–339.

(58) Girifalco, L. A. *J. Phys. Chem.* **1992**, *96*, 858–861.

(59) Hedberg, K.; Hedberg, L.; Bethune, D. S.; Brown, C. A.; Dorn, H. C.; Johnson, R. D.; De Vries, M. *Science* **1991**, *254*, 410–412.

(60) Reith, D.; Müller, B.; Müller-Plathe, F.; Wiegand, S. *J. Chem. Phys.* **2002**, *116*, 9100–9106.

(61) Ghosh, J.; Sun, Q.; Faller, R. Point Dependence and Transferability of Potentials in Systematic Structural Coarse-Graining. In *Coarse-Graining of Condensed Phase and Biomolecular Systems*; Voth, G. A., Ed.; CRC Press: Boca Raton, FL, 2008; pp 69−82.

(62) Hernandez, V.; Casado, J.; Ramirez, F. J.; Zotti, G.; Hotta, S.; Navarrete, J. T. L. *Synth. Met.* **1996**, *76*, 277–280.

(63) Heffner, G. W.; Pearson, D. S. *Macromolecules* **1991**, *24*, 6295–6299.

(64) Mardalen, J.; Samuelsen, E. J.; Gautun, O. R.; Carlsen, P. H. *Solid State Commun.* **1991**, *80*, 687–689.

(65) Ghosh, J.; Faller, R. *Mol. Simul.* **2007**, *33*, 759–767.

(66) Carbone, P.; Varzaneh, H. A. K.; Chen, X.; Müller-Plathe, F. *J. Chem. Phys.* **2008**, *128*, 064904.

(67) Faller, R. *Polymer* **2004**, *45*, 3869–3876.

(68) Piacente, V.; Gigli, G.; Scardala, P.; Giustini, A.; Ferro, D. *J. Phys. Chem.* **1995**, *99*, 14052–14057.

(69) Ballantyne, A. M.; Chen, L.; Dane, J.; Hammant, T.; Braun, F. M.; Heeney, M.; Duffy, W.; McCulloch, I.; Bradley, D. D. C.; Nelson, J. *Adv. Funct. Mater.* **2008**, *18*, 2373–2380.

(70) Li, G.; Shrotriya, V.; Yao, Y.; Yang, Y. *J. Appl. Phys.* **2005**, *98*, 043704.

(71) Moulé, A. J.; Bonekamp, J. B.; Meerholz, K. *J. Appl. Phys.* **2006**, *100*, 094503.